

DLR DESIGN CHALLENGE 2024: DESIGN OF A COST AND ENERGY EFFICIENT REGIONAL AIRCRAFT

Clemens Ehrich¹, Luca Kriebel¹, Tim Schulz¹, Mathias Tekkel¹, Lennart Wauer¹, Leonid Wenz¹, Lucas Kugler², Simon Müller² & Claudio Niro³

¹Institute of Aeronautics and Astronautics, Technical University of Berlin
²German Aerospace Center (DLR), Institute of System Architectures in Aeronautics, Hamburg, Germany
³German Aerospace Center (DLR), Institute of Aerodynamics and Flow Technology, Braunschweig, Germany

Abstract

The eighth edition of the annual DLR Design Challenge, organised by the German Aerospace Center (DLR), invites students of aeronautical sciences to apply, test and demonstrate their knowledge and skills by creatively addressing prospective aeronautical engineering issues and submit an innovative aircraft design. In this year's Design Challenge, students are tasked with designing a future aircraft for operation on European regional routes which is optimised for economical and energy efficiency. By analysing the provided network of routes, the teams can determine their own operational concept and subsequently identify the design point and top-level aircraft requirements, including propulsion technology, design range and passenger capacity. The freedom to select the most appropriate technology and climate-friendly energy source ensures a variety of innovative aircraft concepts for Entry-Into-Service in 2050.

This paper introduces CHARGE, the winner of this years Design Challenge, a narrow body box-wing aircraft with distributed electric propulsion. In response to the significant greenhouse gas emissions of the aviation industry, especially in short-haul operations, CHARGE offers a climate-friendly solution for regional and domestic flights. The aircraft is able to carry 110 passengers over a range of about 900 km, ideal for regional and domestic operation. To enhance operational efficiency and cost effectiveness, CHARGE is equipped with integrated airstairs and an electric nose gear motor for airport independent operation, enabling the aircraft to operate from small regional airports with minimal infrastructure. CHARGE is both energetically and economically superior to its reference aircraft on the given route network, making it a promising and viable concept.

Keywords: education, battery electric aircraft, regional aircraft, box wing, distributed electric propulsion

1. DLR Design Challenge

1.1 Motivation and Objective

The air transport sector will face significant economic and environmental challenges in the coming years. These require innovative and sustainable ideas and approaches in order to offer added value to society. In this context and launched in 2017, the DLR has held an annual competition for students to develop futuristic aircraft concepts that align with current areas of focus in aeronautics research. Most importantly, these designs should embody a coherent overall concept, with a focus on the specific key theme, which changes with each edition. Emerging challenges in aeronautics research, especially in climate change and digitisation, underscore the industry's evolving landscape. These concepts must effectively address critical issues in aircraft design, thereby shaping the future of aeronautical technologies through innovative solutions and visionary approaches. In figure 1 the winning concepts from all editions with their dedicated task are shown.[1]



Figure 1 – History of the DLR Design Challenge

1.2 Organisation

Interested students, who are enrolled at a German university can register in teams through their respective university departments. During the kick-off event at a DLR location, participants are briefed on this year's task and provided with general information about the Design Challenge, along with an introduction to the topic by experts who are dealing with the issue in their research work. The aircraft designs and overall-system concepts are then to be developed over a period of around four months. Once the design reports have been submitted, the Design Challenge culminates in the final event at a DLR location. A jury of DLR experts, consisting of the divisional board member for aeronautics and several institute directors from the field of aeronautics research, is responsible for reviewing and evaluating the aircraft designs. This evaluation is based on the reports and presentations that have been submitted. Finally, the winning teams are announced and awarded.

2. DLR Design Challenge 2024 on efficient regional aircraft design

2.1 Theme

The future of aviation will be climate-friendly. Various projects around the world are aiming to design a net-carbon free aircraft powered by alternative energy sources and revolutionary technologies which enable new possibilities and freedoms for aircraft design. The selection of an aircraft configuration, a suitable propulsion technology, its appropriate integration into the structure and the storage and provision of the energy source are among the greatest and at the same time most exciting challenges of the coming years. However, not only new technologies but also changing boundary conditions are influencing the design of future aircraft. Rising energy and labor costs, coupled with societal transformations, are having an impact on air transport. This effect is especially noticeable at short distances, where the aircraft in use are typically less efficient. According to a DLR study, airline operations on routes shorter than 1,000 km are responsible for more than 30 % of total passenger CO₂ emissions. [2] Therefore, the regional aviation sector must transform to zero-emission operations to remain ecological and economical competitive with other modes of transportation, such as rail and road.

2.2 Task Description

This is where the eighth edition of the DLR Design Challenge comes into play. By considering the forecasted demand on a provided network of 15 highly frequented European regional routes, the objective is to design an aircraft that optimally meets climate and cost efficiency requirements. The participants are asked to design an aircraft for market entry in 2050 that fulfills the task set by combining revolutionary technologies with sustainable energy sources and intelligent operating concepts. The design space is opened up so that the participants can harmonise the mode of operation, propulsion technology and energy source. The aircraft designs are to be optimised for operating costs to guarantee affordable ticket prices while also minimising energy consumption per passenger per kilometre. The detailed task description can be accessed at the Design Challenge webpage.[3]

2.3 Participants and Results

The field of participants is comprised of six teams with a total of 36 students from German universities: DHBW Ravensburg, HAW Hamburg, RWTH Aachen, TU Berlin, TU Braunschweig and University of Stuttgart. As a consequence of the open design space and the necessary network analysis, all concepts differ in terms of their Top Level Aircraft Requirements (TLAR) as well as aircraft configuration as illustrated in figure 2. The concepts vary between a conventional lean hydrogen combustion aircraft designed by the team from Hamburg, a fuel cell powered hybrid blended wing body configuration from Stuttgart and a conventional fuel cell aircraft with boundary layer ingestion (BLI) engine from Aachen. A box-wing configuration featuring a BLI with fuel cells designed by Ravensburg is awarded third-place in the competition. The second-place award is presented to the team from Braunschweig, whose submission is a conventional hybrid-electric aircraft design featuring a range extender powered by sustainable-aviation fuel (SAF). The jury extends its appreciation and recognition to all of the aforementioned submissions. However, the battery-electric box-wing aircraft designed by students from TU Berlin is selected as the winner and is presented in greater detail in the following section. More information about all submissions including reports and pitch-videos can be found in the corresponding press release [4].



DHBW Ravensburg: HYPER



TU Berlin: CHARGE



HAW Hamburg: HydroProp



TU Braunschweig: VoltAirs-95



RWTH Aachen: EcoAir



University of Stuttgart: MOBULA

Figure 2 – Overview of all concepts as part of DLR Design Challenge 2024 (depicted in alphabetical order of university names)

3. Introduction

The challenge of this years DLR Design Challenge entails the creation of an aircraft concept that facilitates climate-friendly short-haul transportation on a specified airport network with a predetermined travel demand. The TLAR of the concept are not strictly defined and with an entry into service (EIS) in 2050, the possibilities for using new innovative technologies are broad. Furthermore the optimal concept and aircraft size has to be based on a given route network and the parameters for optimisation are energy consumption (EC) per seat kilometer and seat kilometer costs (SKC). The proposed solution is **C**arbon-neutral, **H**igh-efficiency **A**ircraft for **R**e**G**ional **E**lectric flight (CHARGE). The following paper will provide an explanation of the aircraft's concept, as well as an analysis of the selected design range in terms of sustainability and economics. An overview is given how the given route network was used to find the optimal aircraft configuration.

4. Market-Concept Analysis

As the aerospace industry and air traffic have struggled during the previous years, the Airbus Global Market Forecast for 2023 shows that air traffic in Europe has recovered fully, compared to 2019 [5]. Traffic flow between central and western Europe is expected to triple already in 2042. Along with

jobs, financial opportunities and future technologies, the impact on the climate must not be forgotten. The *Umweltbundesamt* anticipates a rise in CO_2 emissions of at least $100\,\%$ [6], even though the fuel consumption per revenue passenger kilometer is already decreasing $2.9\,\%$ per year. This illustrates the necessity for the development of novel and innovative aircraft concepts like CHARGE.

4.1 The Search for a New Concept

The European Union has passed the legislation act RefuelEU Aviation to promote the usage of sustainable aviation fuels and make flying in Europe less carbon-intensive [7, 8]. Although these goals are ambitious, they nonetheless extend the timeline for achieving true carbon-neutral aviation beyond 2050. In this timeline, only two energy sources will be available: hydrogen and sustainable aviation fuels (SAF). In contrast, electricity as an energy carrier has a different outlook due to the availability of low-carbon, renewable electricity generation. According to projections, the share of renewable electricity production in 2050 should reach 84 % to 94 % [9, 10]. It can be reasonably assumed that electricity as an energy carrier will be less carbon-intensive than aviation hydrogen or SAF.

A more detailed analysis of the grid-to-shaft energy efficiency of SAF, hydrogen and electricity reveals that electricity as an energy source provides an unbeatable advantage, as demonstrated in table 1. To output $1\,\mathrm{kWh}$ of energy to propel the aircraft using a battery electric powertrain, only an extra $30\,\%$ of energy has to be produced in the grid, compared to over $300\,\%$ for hydrogen and $900\,\%$ SAF. This comparison also extends to the equivalent CO₂ emissions per passenger (PAX)-km, where battery electric aircraft are estimated to emit approximately $5\,\mathrm{g/PAX\cdot km}$, while hydrogen and SAF are found to emit between 50 to $120\,\mathrm{g/PAX\cdot km}$ 1 [11].

Table 1 – Energy pathways for different propulsion systems, Vries et al. [11].

Power-to-lic	uid	synthetic fu	ıel (e	SAF)												
Green electricity		Grid transport ^a		H ₂ electrolysis		CO ₂ direct air capture ^b		e-Fuel synthesis		Transport		Gas turbine				Propulsion
$\rm 5 \sim 9~kWh$	>	94 - 100%	>	70 - 71%	>	63 - 68% or 100%	>	65 - 73%	>	98 - 99%	>	38 - 42%			>	1 kWh
Hydrogen t	urbii	ne														
Green electricity 4 ~ 5 kWh	>	Grid transport ^c 94 - 97%	>	H ₂ electrolysis 70 - 71%	>	Lique- faction 70 - 83%	>			Transport & boil-off ^c 97 - 98%	>	Gas turbine 38 - 42%			>	Propulsion 1 kWh
Hydrogen f	uel d	ell														
Green electricity 3 ~ 4 kWh	>	Grid transport ^c 94 - 97%	>	H ₂ electrolysis 70 - 71%	>	Lique- faction 70 - 83%	>			Transport & boil-off ^c 97 - 98%	>	Fuel cell 50 - 60%	>	Electric motor ^d 85 - 95%	>	Propulsion 1 kWh
Battery elec	ctric															
Green electricity ∼ 1.3 kWh	>	Grid transport 94 - 97%	>				>	Battery charging 95 -96%	>	Battery discharging 95 - 96%	>			Electric motor ^d 85 -95%	>	Propulsion 1 kWh
										← Grid-to-tank	Tai	→ nk-to-shaft				

^a100% if renewable electricity is produced at fuel production site

Both the type of powertrain and the wing configuration also greatly influence the performance and efficiency of the concept. In table 2 an overview of the comparison of different aircraft configuration concepts for the given route network is provided. The different concepts are qualitatively rated based on research of the given literature and the feasibility study described in the section 4.2. The scores are based on projections until EIS in 2050 to find the most promising concept from each category for the defined route network.

A battery electric concept is the most viable solution due to the very high projected availability and low emissions. Here hydrogen concepts have a lower availability score as the produced hydrogen is sorely needed in the industrial sector. The forecast prices for the individual energy sources are

^b100% if carbon is available from elsewhere (e.g., non-clean steel or cement production)

 $[^]c\mathrm{Assuming}$ hydrogen is produced at airport

 $[^]d$ Includes losses of cables, inverters, etc.

¹According to Vries et al. [11], in this CO₂-equivalent the following emissions are accounted for: emissions produced during the mission, emissions generated in the production of the energy consumed during the mission, and emissions produced in the manufacturing of batteries. Emissions generated in the manufacturing process of the vehicle or the infrastructure are not included in this analysis. For in-flight emissions, both CO₂ and non-CO₂ effects are considered, which can be significant.

defined in the assignment, but the total cost listed in the table is based on the results of the total fuels cost estimated in the feasibility study described in 4.2. Only the feasibility of the battery electric concepts is rated lower than the alternatives due to the amount of research necessary into Li-air batteries and how to safely incorporate them in aircraft.

For possible propulsion concepts, distributed propulsion combined with a conventional propeller motor score the best. Ducted fans, whether electric or turbine-powered, also show promise, however, they possess lower efficiency and higher mass. The feasibility for distributed electric propulsion is rated highly, as this topic is currently of high research interest and smaller prototype aircraft are already being developed like the X-57 Maxwell by NASA or the Lilium Jet [12, 13].

For the wing configuration the two most promising options: a strut braced high aspect ratio wing and a box wing (BW) are considered. Both are considered to have a good to very high efficiency and feasibility score. The strut braced wing has a lower score in the operations due to the high wingspan that might limit operation of the aircraft at some smaller regional airports or make the operations in the airport more difficult or time consuming. A BW design can achieve a lower structural mass compared to a strut braced wing, but incurs a penalty for higher complexity for integrating the wing into the aircraft structure.

Table 2 – Comparison of different concepts for energy source, propulsion and wing configuration.

Concept	Parameter								
Energy Source	Availability	System Mass	Efficiency	Feasibility for EIS	Cost (Price)	Total Score			
Battery Electric	++	-	++	+	+ + (0.038 \$/kWh ₂₀₁₉)	7			
Hydrogen	0	+	0	+ +	0 $(0.097 \text{kWh}_{2019})$	3			
Hydrogen Electric Hybrid	0	0	+	++	+	4			
SAF Electric Hybrid	+	+		++	(0.104 \$/kWh ₂₀₁₉)	2			
Concepts for Propulsion									
Propulsion Configuration	System Complexity	Efficiency	Redundancy	Feasibility for EIS	System Mass	Total Score			
Distributed Propulsion	-	++	++	+	+	5			
Ducted Fan	+	+	0	++	0	4			
Propeller	+	+	0	++	+	5			
Concepts for Wing Configu	ıration								
Wing Configuration	Structural Integration	Efficiency	System Mass	Feasibility for EIS	Operations	Total Score			
Strut Braced High Aspect Ratio Wing	+	+	0	++	-	3			
Box Wing	0	++	+	+	+	5			

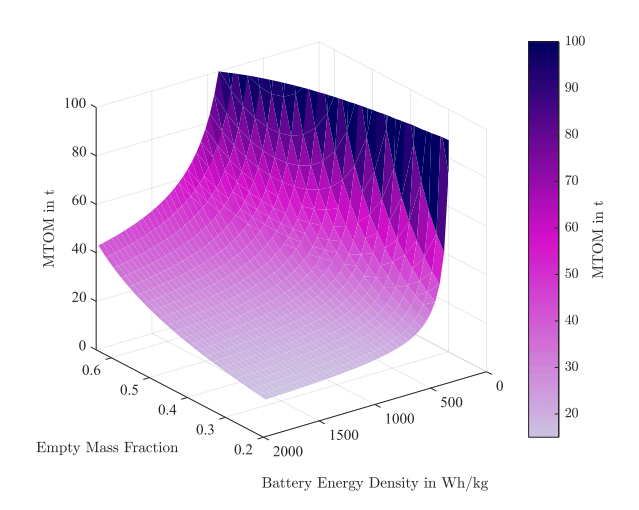
To determine the final configuration, synergies between the single concepts are analysed that can further increase the final efficiency of the aircraft. The energy sources do not have much of a synergy effect with the wing configuration. A SAF electric hybrid would integrate better with a strut braced wing, as the fuel can be more easily stored inside a single wing. A much more important effect is seen in the interplay between energy source and propulsion configuration. Here it is identified that a distributed propulsion concept would integrate well with a battery electric or highly hybridised energy source to allow the use of multiple smaller electric motors spread along the wing. Using this effect it is possible to achieve considerable increases in the efficiency of the aircraft for both wing configurations. Thus, the most promising concept should utilise a battery electric distributed propulsion powertrain combined with a BW.

4.2 Analysis of the given Network

Prior to the detailed design process, a feasibility study was performed to assess the most critical parameters. This includes maximum take-off mass (MTOM), specific Energy (SE) and EC for both a battery electric and hydrogen powered concept based on the required range of $R=1,144\,\mathrm{km}^2$.

 $^{^2}$ longest distance of the indirect route network HAM-EDI with an added diversion range $R_{div}=250\,\mathrm{km}$

This was achieved using the Breguet range equation and methods for energy consumption estimations [14, 15]. The results of the feasibility study for the SE of the battery are presented in figure 3. The diagram shows that the usable SE of the battery should be greater than $500\,\mathrm{kWh/kg}$ to prevent a rapid increase in MTOM with minor alterations to the concept.



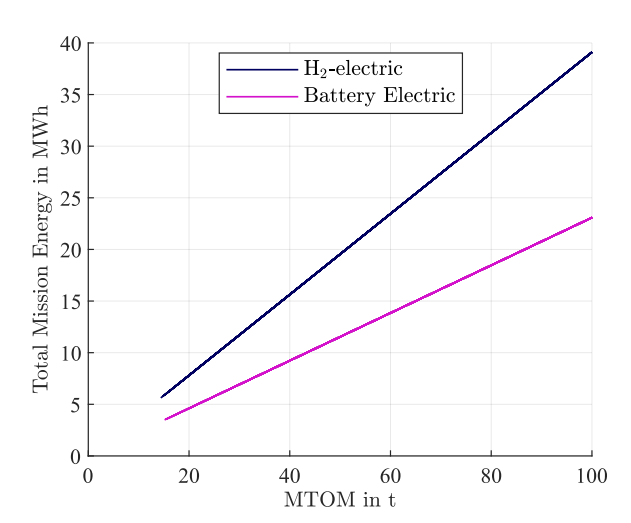


Figure 3 – MTOM over battery SE and empty mass fraction for a range of 1,144 km.

Figure 4 – Comparison of total energy for a battery electric and hydrogen concept for a range of 1,144 km.

Figure 4 demonstrates that an electric powered aircraft with a SE of 1,200 Wh/kg will require less energy to complete a given trip than a hydrogen powered aircraft. The given air traffic network consists of 15 flight connections. The flight range varies between 361 and 1,480 km and can be reduced to 894 km by implementing stopovers. A passenger demand per week is given and must be fulfilled. The indirect flight network is shown in table 8. Further size limiting specifications are the used airport slots in Hamburg, a minimum of 42 slots must be used, a maximum of 276 may not be exceeded. Thus, a design for 60-120 PAX with 4-, 5- and 6-abreast configurations are possible. For each abreast and PAX configuration, it is possible to observe and evaluate the network realisation depending on factors such as cruise speed, turnaround time and a resulting number of planes. The feasibility of size and capacity must be considered carefully. A design for 120 PAX and a 4-abreast configuration has a relatively long fuselage that complicates the BW location, however the desired aerodynamic distance between the two wings does not fit on a short fuselage for 60 PAX - 6 abreast. The complex iteration described in chapter 7 is used to produce flying configurations as shown in figure 5 where the location of the centre of gravity (COG), the area load and the operational decisions of a design are valid.

$$Score = \frac{EC_{max} - EC}{EC_{max} - EC_{min}} \cdot F_{energy} + \frac{SKC_{max} - SKC}{SKC_{max} - SKC_{min}} \cdot F_{cost}$$
 (1)

The designs can be evaluated by introducing a scoring system in which each EC and SKC are ranked from best to worst and are combined to produce a total score calculated using the equation 1. A factor between the two scores can implement the trade-off, whether the design focus is on an environmental or financial optimisation. The primary focus of CHARGE is to reduce EC and thus reduce the total mass and resource usage of the battery. Since operational aspects outweigh airlines' purchase decisions, the impact on direct operating costs (DOC) is not neglected. Thus, the design is optimised with a weighting of 70 % on EC and 30 % on DOC. Figure 5 shows, most of the designs for the indirect connections have better scoring. Limiting the design range results in a lower battery mass and thus in a lower MTOM, which yields a higher efficiency. Also, larger PAX capacities result into less planes needed for network realisation with lower DOC and less total flights and thus a better financial and environmental performance. The best configuration seems to be the 5-abreast - 110 PAX design for the given design range regarding the indirect flight connections.

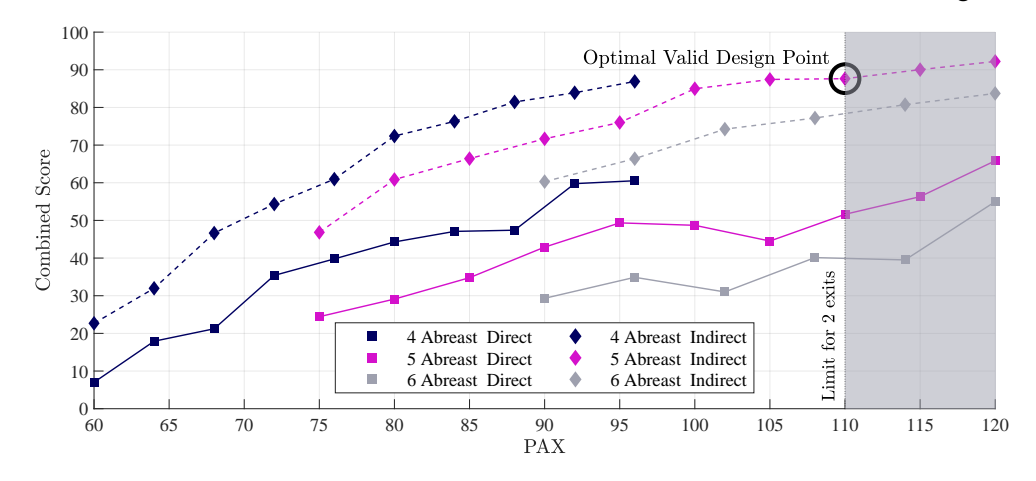


Figure 5 – Scoring of different cabin configurations and PAX values for $Ma_{\rm CR}=0.57$, weighting 70:30 % for EC:SKC.

5. Concept Characteristics

CHARGE builds upon the established tube and wing (TW) concept by integrating a more efficient BW with a sophisticated and efficient battery-powered distributed electric propulsion system. The advantages of the TW concept are maintained by having a versatile and modifiable structure that can easily operate in all airports. As CHARGE is a battery electric aircraft, its CO₂ emissions and operating costs are unbeatable by hydrogen- or SAF-powered alternatives.

Table 3 – Key specifications of the aircraft, powertrain and wing.

Aircraft		Powe	Powertrain			Wing			
Parameter	Value	Parameter	Value	P	arameter	Lower Wing	Upper Wing		
MTOM	39,095 kg	SE _{bat}	1,200 Wh/kg		b	28 m	28 m		
$m_{ m p}$	10,450 kg	m_{bat}	8,924 kg		$h_{ m w}$	5.5 m			
$Ma_{\rm CR}$	0.57	$V_{ m bat}$	$12.17 \mathrm{m}^3$		4	Combined: 98	$.4 \mathrm{m}^2$		
H_{CR}	7,500 m	E_{tot}	12.17 MWh		$A_{ m w}$	$45.4 \mathrm{m}^2$	$53.0 \mathrm{m}^2$		
PAX	110	$P_{ m inst}$	6.24 MW		$lpha_{ m inc}$	2.3°	1.8°		
Seating	5 abreast	$N_{ m motor}$	20		C	Combined: 0.	45		
b	28 m	$\eta_{ m system}$	93 %		$C_{ m L}$	0.55	0.40		
$l_{ m AC}$	30.5 m				Ţ	Total: 383,400	N		
ICAO code	3C	Aircraft P	erformance		L	203,500 N	179,900 N		
$A_{ m w}$	98.4m^2	Parameter	Value		$\Delta_{ m L}$	53 %	47 %		
$C_{ m L,CR}$	0.45	TOFL	1,410 m		$arphi_{ m LE}$	30°	-27°		
$C_{ m D,CR}$	0.16	LFL	1,303 m		λ	0.4	0.35		
R	894 km	$c_{ m IC,max}$	6.7°		Γ_3	5°	− 4°		
(G/F)	$3,896 \text{N/m}^2$								

The box wing, also known as a Prandtl wing was proposed in 1924 by Ludwig Prandtl as a configuration with low induced drag and thus high efficiency [16]. A BW resembles a biplane from the front, but from the side it is noticeable that the lower and upper wings are offset in the longitudinal direction and connected at the tips by winglets. The winglets act as barriers to reduce the strength of the vortexes formed at the tip of the wings. As an effect, the induced drag is considerably reduced. The wings can achieve a more uniform lift distribution along the wingspan and thus a higher wing load as visible in figure 14. To further increase efficiency, the upper wing is positioned above the V-tail to increase the vertical distance between the wings. Another effect of the connected wings is their structural stability as the forces and moments created by the aerodynamic forces do not have to be carried by a single wing root, but are transferred over the vertical elements and shared by both wings. The forces and

³The positive dihedral angle is for the lower wing and the negative anhedral angle for the upper wing

moments on the upper wing are carried into the fuselage structure over the V-tail. This also reduces the total weight of the wings, although the aerodynamic loads near the tips of the wings are higher compared to a conventional wing. As a positive effect the Operating Empty Mass (OEM) of a BW aircraft can be lower then a conventional TW configuration with the weight savings coming from the lower combined weight for the fuselage and wing group [17].

CHARGE is equipped with a distributed electric propulsion (DEP) system on both the upper an lower wing. As a result, this concept benefits from higher propulsion efficiency, lower noise emissions and improved low-speed characteristics. CHARGE is a full-electric aircraft and there is no need for a hydraulic or pneumatic system. All systems are powered by the four lithium-air battery packs incorporated into the fuselages underfloor section. To control the aircraft, a combination of the ruddervators in the V-tail, the control surfaces on both wings, the horizontal morphing wing rudder and differential thrust of the DEP system is to be used. Combining the high aerodynamic efficiency and lower structural mass of a BW leads to a configuration that can achieve the necessary lift and efficiency with a lower wingspan than conventional configurations. This gives CHARGE an important advantage when operating in the proposed route network with mostly smaller regional airports as the wingspan of the aircraft b of $28 \, \mathrm{m}$ is classified as ICAO Class C ($24 \, \mathrm{m} < b < 36 \, \mathrm{m}$) [18] and suitable for all the proposed airports. The $28 \, \mathrm{m}$ wingspan allows CHARGE to move and use all facilities at airports without obstacles. The C classification will also reduce fees as the aircraft can use smaller parking stands. The three sided view of CHARGE is shown in figure 6. All key specifications are summarised in table 3.

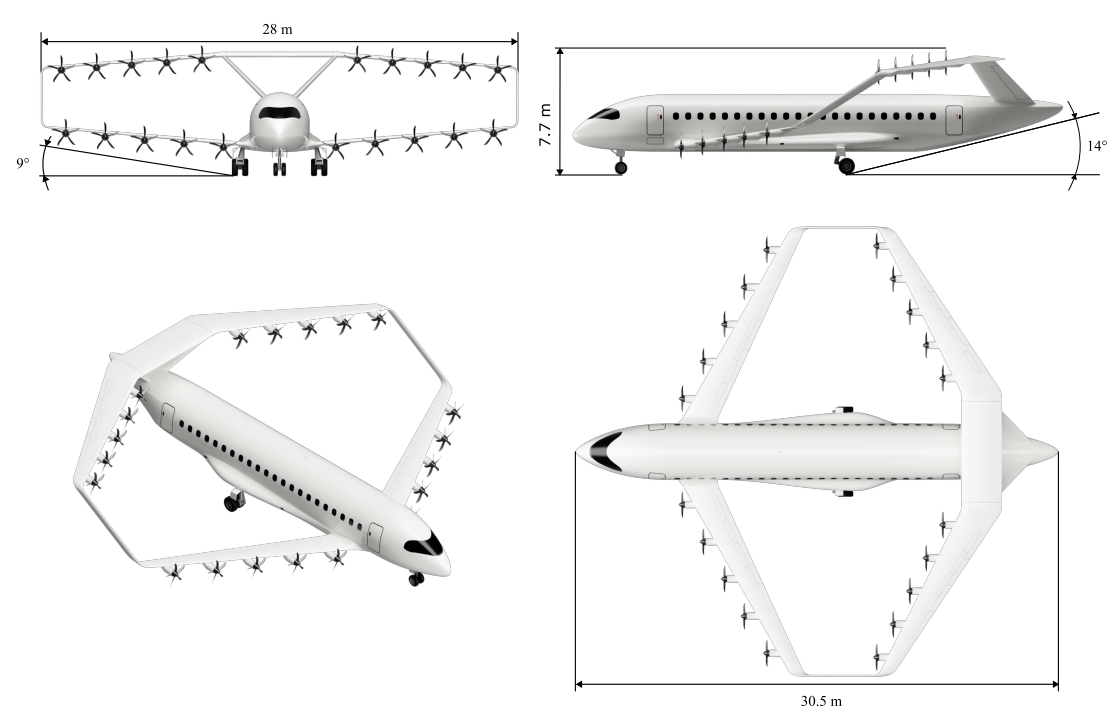


Figure 6 – Three sided view of aircraft.

5.1 Mass Estimation

The chosen PAX capacity and design range but also the aircraft configuration are key aspects which influence the mass estimation. Most of the detailed evaluation can be performed, using statistical methods of Torenbeek [19], Raymer [20], Nicolai and Carichner [21]. As a structural wing concept would be too complex to design, the wing is considered as two separate wings, each lifting part of the total aircraft mass. Additionally, two connecting winglets for structural support are taken in account of. For the structural benefits of a BW configuration, realised by use of modern composite structures, a conservative reduction of $20\,\%$ is made. For the fuselage, landing gear and surface control group, Raymer suggests technology factors for structural mass reduction of $10\,\%$, $5\,\%$ and $40\,\%$. A detailed mass estimation is shown in table 4.

Table 4 – Breakdown of mass estimation.

Group Indication		Mass in t	% of MTOM
Airframe Structure	Wing Group	6.00	15
	Fuselage	3.72	10
	Tail	0.31	1
	Landing Gear	1.55	4
	Surface Control	0.58	2
	Group Total:	12.16	31
Propulsion Group	Motor, Propeller & -control, Inverter, etc.	1.29	3
Electrical Group	Actuators, Cables & misc.	1.66	4
Airframe Services & Equipment	Instruments, Furnishing & Equipment, etc.	3.26	8
Delivery Empty Mass (DEM)		18.37	47
Operational Items	Safety, Seating, Provisions, etc.	1.36	3
OEM		19.72	50
Payload		10.45	27
Zero Battery Mass (ZBM)		30.17	77
Battery Mass		8.92	23
MTOM		39.10	100
Max. Battery Mass Increase	(for Holding (HLD) & Alternate (ALT))	0.61	2
Maximum Landing Mass (MLM)		39.72	102

5.2 Aircraft Systems

This section presents the individual aircraft systems, their concept design and integration. As CHARGE is a full electric aircraft, the propulsion system depends on electric motors, power electronics and of course a battery system. Furthermore this concept does not rely on any hydraulic or pneumatic system but instead utilises electric actuators and an electric environmental control system (ECS). The placement of all different Aircraft Systems is illustrated in figure 7.

5.2.1 Distributed Electric Propulsion System

DEP is a variant of a propulsion system in which the thrust is distributed across the span of the aircraft's wing by a number of electric propulsion units. A well-designed DEP system offers several advantages over traditional propulsion systems. One of the key benefits is an enhanced aerodynamic efficiency that mainly results from an increase in the total disc area A_{Prop} compared to similar traditional propulsion systems [22]. This causes the additional effect of reduced noise emissions [22]. In particular, during low-speed flight, the aircraft is able to maintain greater rudder authority due to the accelerated airflow around the wings. At the same time, this increases the effectiveness of the high-lift devices, resulting in a shorter, take-off and landing distances.

In order to make use of and quantify these potential advantages, a detailed analysis of the aero-propulsive interaction is mandatory [22, 23]. Such an analysis is not feasible for a concept design. Therefore HEPPERLE [23] proposes a method to asses the most important design parameters, such as the number of engines, propeller diameter and engine position. The general idea behind this method is to compare the total disc area $A_{\rm prop}$ of the DEP system to a reference aircraft, in this case the De Havilland Canada Dash 8 Q400 (Dash 8). A similar total disc area leads to approximately the same propulsion efficiency $\eta_{\rm prop}$, while choosing a larger total disc area improves the overall efficiency [23]. Assuming the motors are evenly distributed over the entire wingspan, increasing the number of motors $N_{\rm motor}$ results in a smaller total disc area. So using fewer motors should in theory result in a greater efficiency. At the same time lowering the number of motors increases the total system mass because of the larger propeller diameter $d_{\rm prop}$ [23].

Considering the total disc area $A_{\rm prop}$, but also the system mass and complexity, an optimal number of propulsion units for CHARGE was determined to be twenty, of which ten are located on each wing. There are no propulsion units placed on the morphing trim area between both V-Tails, as the motor fairing would interfere with the morphing structure. For reasons of simplicity in design and production,

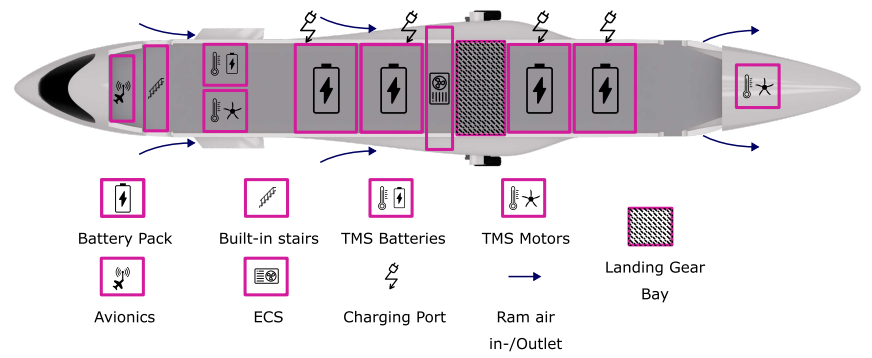


Figure 7 – Display of most relevant aircraft systems.

all propulsion units use the same diameter for the propellers. This leads to slightly different tip to tip distances for lower and upper wing, due to different usable wingspans. The propeller diameter is chosen so that sufficient clearances are maintained between the propeller tips, fuselage and ground. The configuration above ensures a total disc area A_{prop} 1.8 times greater than the reference aircraft, while the total system mass is 34% lighter [24, 25].

In addition to the number of motors, the positioning on the wing also has a decisive influence on the system efficiency [23]. It is desirable to position the propellers in a location where the local flow velocity is as low as possible [23], which is usually below the wing. The engines of CHARGE are positioned under the wing in such a way that this effect is utilised as far as possible without the drag of potentially extended engine nacelles leading to greater efficiency losses than are gained by the placement. To account for the positive effects of a DEP in the aircraft performance calculations, it is assumed that CHARGE is able to perform its takeoff in 10% less distance compared to the standard configuration which is a conservative estimation [26]. Aside from the better take-off performance, there is a higher efficiency expected in cruise due to the high total disc area compared to the Dash 8.

5.2.2 Propulsion Unit

Each propulsion unit consists of a five-bladed propeller and the nacelle accommodating the Motor and Inverter as shown in figure 8. The specific power (SP) for the motors are assumed to reach $16 \, {}^{kW}/{}_{kg}$ by 2050 using advanced super conducting high efficiency technology currently developed by National Aeronautics and Space Administration (NASA) with a proposed efficiency η_{motor} of 99 % [27]. To give each propulsion unit the ability to be controlled individually, and for reasons of high redundancy, each motor is equipped with its own inverter with a SP of $20 \, {}^{kW}/{}_{kg}$ at 99.5 % efficiency $\eta_{inverter}$ [28]. This additionally enables the propulsion system to implement thrust vectoring abilities. The propeller system incorporates a pitch control system to ensure maximum propulsion efficiency in all phases of flight. The tip speed of the propellers is kept similar to that of the reference aircraft, resulting in a speed n_{prop} of 2,440 rpm. This propeller speed is adjusted to the engine speed with a small gearbox, which is installed between the engine and propeller. The engine speed n_{motor} is expected to be approximately $6,000 \, \mathrm{rpm}$, resulting in a gear ratio $i_{gearbox}$ of 1/2.5.

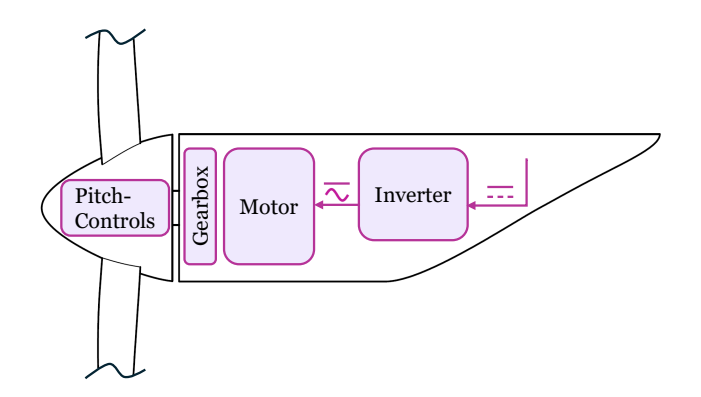


Figure 8 – Schematic of the propulsion unit.

Table 5 – Propulsion parameters.

Parameter	Value	Source
SP Motor	16 kW/kg	[27]
$\eta_{ m motor}$	99 %	[27]
SP Inverter	$20 kW/\mathrm{kg}$	[28]
$\eta_{ ext{inverter}}$	99.5 %	[28]
d_{prop}	1.7 m	-
$n_{\rm prop}$	2,440 rpm	-
$n_{ m motor}$	6,000 rpm	-
$i_{ m gearbox}$	1/2.5	-
$A_{\rm prop}$	46.3m^2	-

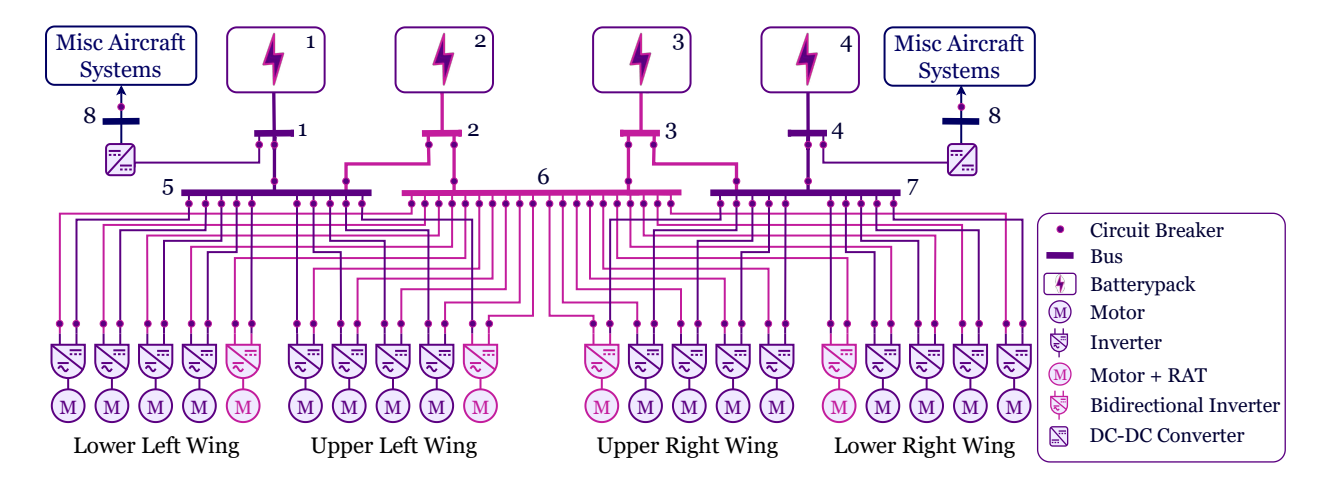


Figure 9 – Schematic of the power distribution architecture.

5.2.3 Power Distribution

With the all-electric architecture of CHARGE, power distribution is a key aspect of the design process to ensure safe and efficient operation. The power distribution is based on a three-bus multi-feeder architecture as shown in figure 9. This layout provides an excellent redundancy while maintaining light weight [29].

All motors are directly connected to two independent buses, while each main bus (five to seven) is directly powered by two battery packs. This ensures that in the event of any single failure other than a direct motor failure, all motors can still be powered via an alternative route. The failure modes considered are direct battery pack failure, any random bus failure, and any cable failure. All cables, batteries and buses are sized for the corresponding worst case failure as described. In case of a severe electrical failure or the unlikely event of completely drained batteries, all inboard propulsion units are able to act as ram air turbine (RAT) and feed electricity back into the most critical systems such as the actuation system of the flight controls and avionics. Due to a higher potential system efficiency $\eta_{\rm sys}$, the whole power distribution system is based on variable system voltage (VSV), which means that the decreasing battery voltage is not compensated for by converters, but rather is fed directly into the consuming systems [30]. The design system voltage is defined at 0 % state of charge (SOC).

The high power demand of all-electric aircraft would lead to unbearably high currents with today's voltage level standards [31]. System voltages in the kilovolt range are necessary to enable efficient energy transport through the aircraft. Determining an optimal system voltage requires a detailed sensitivity analysis using the system masses and efficiencies [32]. For the preliminary design, 4kV has been identified as a suitable system voltage V_{sys} on the basis of several studies [30, 33]. High voltage present a number of challenges. One of which is the higher risk of arcing at high voltage and altitude, which sets high requirements for cable insulation and routing [33]. To address some of these challenges, CHARGE uses advanced micro-multilayer multifunctional electrical insulation (MMEI) [34]. Hereby multiple functions are incorporated into the insulation by combining different materials with different properties [34]. Another challenge when using high voltages is the safe and reliable disconnection of loads under load and in case of a fault. Therefore 95 circuit breaker (CB)'s are distributed along the power grid as shown in figure 9. The assumed SP of the CB's is $200 \, kW/kg$ at 99.9 % efficiency [35] For all smaller non-propulsive loads a 1 kV bus is utilised and fed redundantly from packs one and four. These loads consist mainly of the actuation system, wing-ice protection system (WIPS), E-taxi system, lighting and galley loads. All avionics are powered from an additional 28 V bus and therefore meet today's standards. There is a total of 477 m high voltage cable routed through CHARGE. The cross-sections are estimated according to DIN EN 2853 [36] adjusted for aluminium as conductor. The individual cable and CB masses and positions are being considered in the mass estimation and determination of the COG.

5.2.4 Battery System

As seen in figure 3, the whole concept is dependent on sufficient SE of the batteries. Because of the high theoretical SE the batteries are chosen to be Li-Air. The cells consists of a lithium-anode and air-cathode separated by a solid electrolyte [37]. The chemical reaction appears as follows:

$$2Li + O_2 \longrightarrow Li_2O_2$$
 (Discharge) (2)

$$\text{Li}_2\text{O}_2 \longrightarrow 2\text{Li} + \text{O}_2$$
 (Charge) (3)

with the oxygen provided by the air [37]. Due to the chemical reaction, the battery mass m_{bat} and volume V_{bat} increases during discharge mid-flight. The lithium binds added oxygen as seen in 3. The operating mechanism of the battery shows an increase of 0.1 g/wh. The volume increase is taken into account in the pack architecture as the needed volume is calculated for the discharged case. During discharge, additional oxygen is needed inside the cells, this is ensured by air flow provided by the four ram air inlets shown in figure 7. A total of approximately 11,700 m³ of oxygen are required for the longest flight. Given that the batteries are supplied with ram air the inlets are sized for the most critical combination of required battery power and occurring dynamic pressure. This is the case at the start of the climb segment during acceleration to cruise speed. The required volumetric flow $\dot{V}_{\rm max}$ amounts to $1.35 \, \text{m}^3/\text{s}$. During takeoff the batteries are supplied with compressed air from the ECS to account for the low ram pressure. A SE of 1,200 Wh/kg [32] and energy density of 1,000 Wh/L [38] are used. Due to 20% depth of discharge (DoD) protection and 20% degradation over lifetime, the effective SE is only 720 Wh/kg [39]. The batteries are split up into four packs, separated from each other, due to safety precautions. Each pack can be charged with one charging plug. Discharge and charge efficiencies (η_{charge} , $\eta_{\text{discharge}}$) are both 95 % [11]. A maximum SP of 917 W/kg is required during discharge, which translates to approximately $0.7\,\mathrm{C}$ at $2.96\,\mathrm{V}$ cell voltage V_{cell} [40]. A charging power $P_{\rm charge}$ of 3,000 kW at 4 kV, which is also the system voltage $V_{\rm sys}$, as described in section 5.3s used, resulting in 1 C during the charging process. The lifetime of the cells is expected to be 1,500 full cycles [11]. At the end of their lifetime the packs are removed through access panels and replaced. Beside technical requirements the batteries need to ensure safety standards. In contrast to Li-Ion cells, thermal rundown due to overcharge is no concern with the Li-Air chemistry [37]. Although a fire is very unlikely an extinguishing system is installed. In case of fire, a powder is injected directly inside the pack to contain the flames. In addition, the pack is disconnected from the system and cooled until a safe landing and evacuation at the nearest airport is executed.

5.3 Thermal Management System and Environmental Control System

To achieve the highest possible energetic efficiency, CHARGE implements an integrated architecture of all thermal and environmental systems. Meaning that the ECS is able to utilise the excess heat from the thermal management system (TMS) and can allocate this heat to the WIPS and cabin if needed [41]. Furthermore the ECS works based on a design not relying on bleed air with an assumed power consumption of $68.4\,\mathrm{kW}$ during climb and descent and $42.8\,\mathrm{kW}$ in cruise flight [42]. The resulting energy usage is considered into the energy calculations in section 5.9The TMS consists of three independent cooling loops. This is due to different operating temperatures and positions in the aircraft [43]. The lower and upper wing each use a separate cooling loop which is supplied by ram air from the inlets located at the lower wing fairing and belly fairing. The third cooling loop is used to keep the battery at an optimal operating temperature. A SP of $3\,\mathrm{kW/kg}$ for all cooling systems is assumed [44]. The actual TMS mass is therefore determined by the loss of each cooled system. The power consumption of the TMS itself is approximated with $1.5\,\mathrm{W/kg}$ [44]. It is also possible to preheat the batteries in case of cold temperatures during ground time. The energy is provided via the charging ports.

5.4 Structural Design

As visible in figure 6 the main gear is not located in the lower wing box, but is placed in the middle of the fuselage in a separate fairing, much like a typical high-wing aircraft. When the gear is retracted, it is stowed completely inside the fairing. The frame extends up to the lower wing box and houses

much of the equipment for ECS. The aerodynamic shape of this fairing also allows it to act as a lifting body, creating lift to compensate for the slightly increased drag. The structural design of the fuselage is shown in figure 10. The fuselage structure is a semi-monocoque carbon fibre reinforced plastic (CFRP) sandwich composite.





Figure 10 – Structural concept of fuselage.

Figure 11 – Sandwich structure with keel beam.

The outer shell of the fuselage is composed of two layers of CFRP with a sandwich structure between them (colored yellow in the figure). This allows omitting the stringers in the fuselage structure without compromising the stiffness and strength of the structure. In the lower part of the fuselage, a keel beam made of CFRP is integrated directly into the sandwich hull structure. The fuselage is made of sections, each section being $1,524\,\mathrm{mm}$ long and spanning two windows. On the inside, frames running around the fuselage connect the transverse floor frames to the outer hull. Running longitudinally from the front to the rear of the structure, the floor beams are positioned under the seat tracks of the 3-2 abreast configuration. On the right side of the fuselage the openings for the doors, to access the batteries are visible. The structures pointing out of the fuselage on the right side are attachment points for the main gear and the V-tail. For a better overview the wing box for the lower wing is not shown. The calculated shear force on the wing box for the lower wing is $V_{\mathrm{lower}} = 80\,\mathrm{kN}$ and the root bending moment $M_{\mathrm{lower}} = 429\,\mathrm{kNm}$. The upper wing attached to the V-Tail experiences a shear force of $V_{\mathrm{upper}} = 81\,\mathrm{kN}$ and a root bending moment of $M_{\mathrm{upper}} = 520\,\mathrm{kNm}$.

5.5 Cabin and Fuselage design

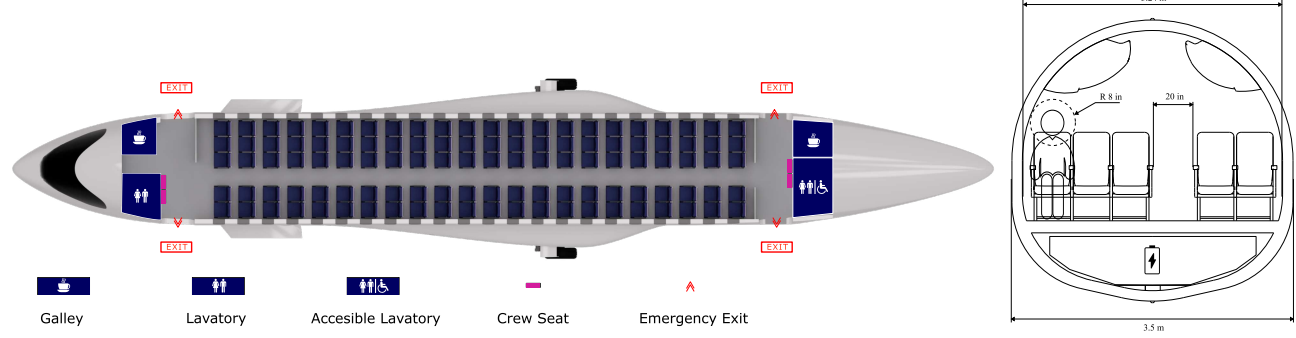


Figure 12 – Cabin layout.

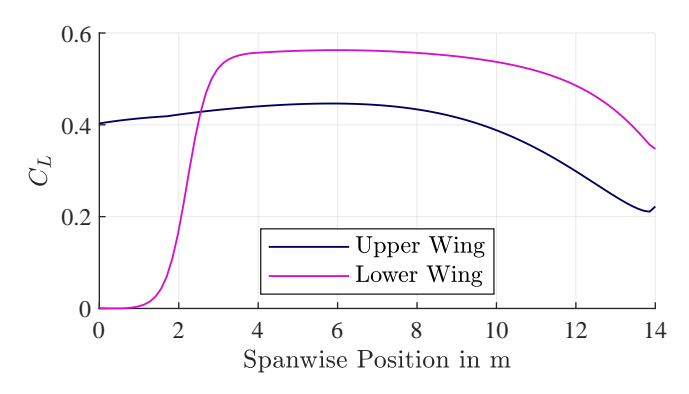
Figure 13 – Cabin cross section.

CHARGE is designed to accommodate 110 PAX in a 5-abreast all-economy layout, figure 12. A seat pitch of $30\,\mathrm{in}$ plus galleys, lavatories and emergency exits results in a cabin length l_cab of $22.12\,\mathrm{m}$. To improve passenger comfort and operational flexibility, CHARGE is equipped with two lavatories. The additional lavatory ensures the operation of the aircraft even if one lavatory becomes inoperative. Two galleys capable of holding a total of five full-size-trolleys are installed in the front and back of the aircraft. The 5-abreast seating configuration dictates a cabin width d_cab of $3.24\,\mathrm{m}$, resulting in an overall fuselage diameter d_fus of $3.5\,\mathrm{m}$. As shown in figure 13, the fuselage cross-section is adapted from a circular shape, with a widened lower half to accommodate the aircraft's batteries.

All aspects of the cabin design comply with CS-25 regulations, such as maintaining an eight-inch head impact radius on hard monuments and minimum aisle width as shown in figure 13. CHARGE is equipped with two pairs of Type A sized emergency exits, enhancing the comfort of embarkation and disembarkation. For operational efficiency, these exits are certified as Type C, reducing the number of cabin crew required without compromising safety. Each pair of Type C exits is certified for 55 PAX, giving the aircraft a total maximum PAX capacity of 110, requiring three cabin crew.

5.6 Aerodynamics

To calculate the aerodynamic characteristics of the BW it is necessary to divide the wing into a lower and upper surface and calculate the aerodynamic characteristics separately. The calculations from SCHIKTANZ [45] and FINCK [46] are used to take into account the effect of the forward lower wing on the lift and moment coefficient of the aft upper wing. The increase of aerodynamic efficiency in a BW-design is due to the reduction of the vortex strength at the wing tips, because of the continuous vertical winglets. The reduced vortex strength decreases induced drag while increasing the lift distribution around the wing tip. The effect in efficiency is twofold by reducing drag and at the same time increasing lift. This effect is strongly influenced by the vertical stagger $h_{\rm w}$ of the single surfaces and the difference in the lift forces acting on the single surfaces [47]. For an exact calculation of the efficiency factor without comprehensive computational fluid dynamics (CFD)-simulations estimations according to RIZZO [48] were used in an iterative loop, taking into account the changes in geometry and aerodynamic forces.



$$\gamma(\eta) = \gamma_a(\eta) \cdot c_L + \gamma_b(\eta) \tag{4}$$

$$\gamma_a(\eta) = c_1 \frac{l(\eta)}{l_m} + c_2 \frac{4}{\pi} \sqrt{1 - \eta^2} + c_3 \cdot f(\varphi, \eta)$$
 (5)

$$\gamma_b(\eta) = k_1 \cdot c_L' \cdot \gamma_a(\eta) \cdot \left[\varepsilon(\eta) - \int \varepsilon(\eta) \cdot \gamma_a(\eta) \, d\eta \right]$$
(6)

$$K = \frac{e \cdot \Lambda}{\frac{c_L'}{2\pi} \cos \varphi_{25}} \tag{7}$$

Figure 14 – Lift distribution along the lower and upper wing along the wing span.

In order to take into effect factors like the wing sweep and taper ratio, the lift forces along the wingspan were calculated using the method by DIEDERICH for subsonic speeds [49]. The first component of the circulation distribution γ_a in the equation 4 consists of the sum of an ellipse, depth and dihedral function and the second component γ_b in 4 describes the effect of wing twist. Both components for γ are dependent on coefficients C that can be calculated using a polynomial approximation. For brevity the coefficients are not further explained. It is important to note, these coefficients are dependent on the factor K (7), describing the form factor of the wing. To take into account the increased efficiency of the BW, the original formula for 7 is multiplied with the Oswald factor e. It is of note, that the calculated value for e = 1.4 exceeds 1, an effect unique to the BW.

The result of the span wise lift distribution of one side can be seen in figure 14. The distribution of the lower wing starts with a value of 0 and reaches a nominal value by $2.5 \,\mathrm{m}$ to consider the effect of the body, where the wing and its lift generation are interrupted. The high C_L value at the tips of the wings correspond to the expected effect of a BW and are comparable to the results in SCHIKTANZ [45] and PALAIA, ABU SALEM, AND QUARTA [17].

To calculate the total drag, a multiprong approach was used. The distribution of the drag components is displayed in figure 15 The wing drag is calculated using the known lift distribution along the wingspan together with the local wing depth and is calculated for the upper and lower wing separately by using equation 8. To approximate the total wing drag it is necessary to divide the drag components

into skin friction and pressure drag. It is noteworthy to note that, although it is customary to estimate a proportion of the airflow around the wing as laminar, this positive effect could not be relied upon for this concept due to the effect of the DEP on the wing inflow.

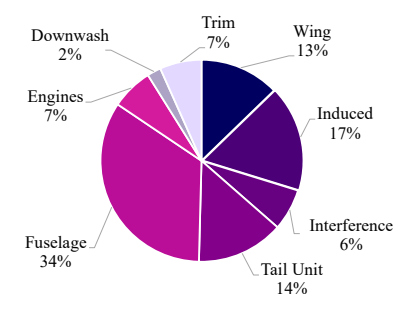


Figure 15 – Detailed drag breakdown.

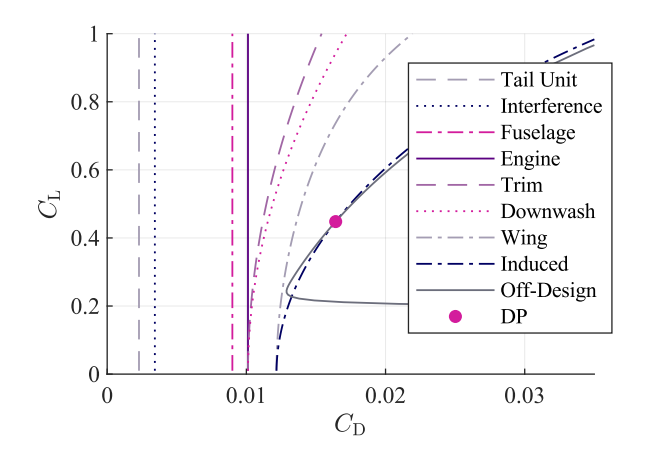
$$C_{\mathrm{D,W}} = \int C_{\mathrm{D,W,min}} + 0.03 \cdot C_{\mathrm{L}}^{6}(\eta) \cdot \frac{l(\eta)}{l_{\mathrm{MAC}}}$$
 (8)

$$C_{\mathrm{D,W,min}} = 2 \cdot C_{\mathrm{f}} \cdot (1 + k_{\mathrm{W}} \cdot \cos \varphi_{50}^2) \tag{9}$$

$$C_{\mathrm{D,i}} = \frac{C_{\mathrm{L}}^2}{\pi \cdot e \cdot A_{\mathrm{W}}} \tag{10}$$

$$C_{\text{D,int}} = \sum_{i=1}^{n} \frac{\frac{0.1369}{\text{Re}^{0.4}} \cdot l_{\text{intersection}}^{2} \cdot n}{A_{\text{w}}}$$
 (11)

Therefore, the minimum wing drag is calculated in accordance with the estimations proposed by DIEDRICH in equation 9, whereby the coefficient of friction $C_{\rm f,tu}$ is dependent on the Reynolds number Re, while the pressure drag coefficient $k_{\rm W}$ is dependent on the length-thickness ratio. A similar, simplified calculation is employed for the tailunit drag coefficient $C_{\rm D,T}$. The final significant component-independent drag coefficient is the interference drag $C_{\rm D,int}$. This is approximated by applying equation 11, where n represents the number of analogous intersections between sub assemblies. Whereas $l_{\rm int}$ describes the interferences length.



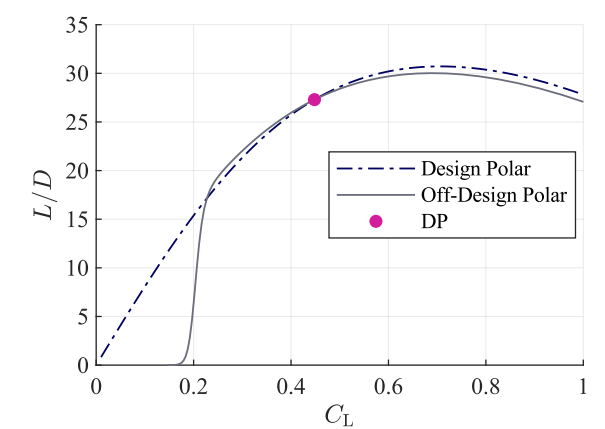


Figure 16 – Cumulative drag polar.

Figure 17 – Lift to drag polar.

The drag for the other components also visible in figure 16 is calculated using approximations based on calculations carried out by DIEDRICH as well, wich are presented by TORENBEEK [19]. They all depend on some variation of skin friction and pressure drag. The final Design Point (DP) results in a lift coefficient of $C_{\rm L}=0.4480$ and a drag coefficient of $C_{\rm D}=0.0152$. This yields a lift to drag ratio of $L/D\approx27$. This DP results in a stable configuration during cruise, as shown in figure 17.

5.7 High Lift Devices and Surface Controls

CHARGE is able to control its flight attitude through various control surfaces and its propulsion system, as seen in figure 6. The roll movement is realised by the outboard ailerons on both wings trailing edges. The morphing trailing edge rudder [50] on the horizontal surface between both V-tails enables the aircraft to change the generated lift of the upper wing without creating downforce. This is used to on the one hand trim the aircraft in the most efficient way but also acts as elevator. The DEP system enables CHARGE to create yaw movement by inducing an intentional imbalance in thrust. This differential thrust is more efficient than ruddervator movement [15]. For large pitch and yaw adjustments and for redundancy reasons the V-tail of CHARGE is also equipped with conventional ruddervator surfaces.

The V-tail has a projected horizontal area of $17.4\,\mathrm{m}^2$ and a distance between the aerodynamic centre of wing and V-tail of $10.6\,\mathrm{m}$. Thus, a horizontal stabiliser volume of $184.3\,\mathrm{m}^3$ is achieved, $73\,\%$ of the reference planes horizontal stabiliser volume.

During descend or deceleration it may be necessary to increase the drag of the aircraft. Therefore both wings of CHARGE are fit with a spoiler system that can be deployed when needed. During low speed CHARGE profits from the DEP's increased airflow around the wings. However, this effect is not sufficient to fulfil the take-off and landing requirements. Therefore CHARGE is equipped with a high lift system on both wings. This system is a combination of a morphing droop nose and a fowler flap on the trailing edge. While the trailing edge devices are constructed in a traditional way, the morphing droop nose is an aerodynamically efficient way of increasing the maximum lift coefficient of the wing while reducing noise emissions compared to a conventional slat [51].

5.8 Aircraft Balance



Figure 18 – Location of COG.

The location of the aircraft's COG has a massive influence on its flight mechanical behaviour. Therefore, a detailed analysis of the mass distribution of CHARGE was carried out to position the overall COG 10% in front of the overall aerodynamic centre to ensure statically stable flight behaviour. Due to the nature of the BW the wing position is not as easy to adjust as on traditional wing concepts, which can make meeting this requirement a challenge. This is mainly due to the upper wing being connected to the tail structure and thus being restricted in its position. While the distance between the wings as well as the whole tail section with the upper wing can be altered to move the aerodynamic centre, other constraints like the battery position between the wings and exit locations also need consideration. The positions of the COG and aerodynamic centre are illustrated in figure 18.

5.9 Aircraft Performance

The results of the calculations provide a design space in terms of take-off wing loading $(G/F)_{TO}$ within which a valid design can be realised, as seen in figure 19. This design space is further constrained by the landing requirements. All power requirements (P/G) are calculated using the methods proposed by PALAIA [52]. Due to the lack of public data on thrust characteristics of modern propeller systems, assumptions must be made about the efficiency of the propellers. It is therefore assumed that the efficiency of the propellers is $\eta_{\text{Prop},CR} = 85\,\%$ in cruise flight and $\eta_{\text{Prop},TO} = 75\,\%$ during take-off and initial climb. The performance requirements refer to the shaft power of the motors.

The required take-off power is mainly influenced by the Take-Off Field Length (TOFL) and the maximum lift coefficient in takeoff configuration $c_{\rm L,max,TO}$. Due to the positive influences of DEP, CHARGE is able to perform the take-off in $10\,\%$ less distance than a conventional propulsion system design. Consequently, to achieve the demanded TOFL of $1,510\,\mathrm{m}$, less thrust is required. The take-off calculations were made in compliance with CS 25 using methods from Palaia [52] and Sforza [53].

The design cruise altitude H_{CR} for CHARGE is selected so that flights over mountain ranges such as the alps are possible. The operational cruise altitude can however be adapted to each flight mission. The most efficient descent is conducted at best glide speed $v_{a,min}$. However, as for CHARGE this flight speed is on average $120\,\mathrm{m/s}$, this would lead to a very long and time consuming descent. For normal operation this is not practical. Therefore CHARGE descends with a predefined profile of Ma 0.57 or $270\,\mathrm{kts}$ indicated airspeed (IAS) whichever is lower at given height. Below $10,000\,\mathrm{ft}$ the descent speed is reduced to the regulatory maximum of $250\,\mathrm{kts}$ IAS. All motors are feathering during descent, thus no energy is used by the propulsion system and the drag is minimised.

DLR Design Challenge 2024

Table 6 – Performance parameters.

30 Take-Off Cruise	
Z 25 - Climb AEO 4° Climb OEI CS 25.121 Approach Climb CS 25.121	
Go-Around CS 25.119 Maximum LFL	
Climb AEO 4° Climb OEI CS 25.121 Approach Climb CS 25.121 Go-Around CS 25.119 Maximum LFL Minimum Approach Speed Feasible Design Space DP	
ot 10	
de Mood 5	
0	
1000 1500 2000 2500 3000 3500 4000 4500 5000 Wing Loading at Take-Off in $(G/F)_{TO}$ in N/m ²	5500 6000

Parameter	Value
TOFL	1,410 m
$\eta_{ ext{Prop}, ext{TO}}$	75 %
$C_{ m L,max,TO}$	2.2
P_{TO}	5.45 MW
$c_{IC,max}$	6.6°
mean ROC	$6.38\mathrm{m/s}$
$\eta_{ ext{Prop,CR}}$	85 %
P_{TO}	$3.02\mathrm{MW}$
mean ROD	$6.72\mathrm{m/s}$
Descent Profile	Ma 0.57/270 kts IAS
v_{APP}	64.1 m/s
a_{APP}	6.74°
$C_{ m L,max,LDG}$	2.8
LFL	1,303 m
$s_{ m LDG}$	782 m
$(G/F)_{TO}$	$3,896\mathrm{N/m^2}$
$P_{ m inst}$	6.24 MW

Figure 19 – Power requirements as a function of wing loading at take-off.

This compromise ensures both a time and energy efficient descent with the added benefit of reducing noise emissions. The relevant performance data is summarised in table 6. Below 1,000 m, again due to noise reducing measures, CHARGE is able to maintain a descent angle of more than 5.5°. This angle is lower than the glide angle a_{APP} which means no additional lift reducing measures like spoilers are necessary to be deployed apart from possible deceleration phases. According to CS 25.119 and CS 25.121 the aircraft has to achieve certain climb gradients in case of an approach climb or go around. This results in additional power requirements that were considered during the design process and are shown in figure 19. In terms of wing loading G/F there are two boundaries relevant at landing for the design of CHARGE. The first boundary results from the given maximum landing field length (LFL) of 1.510 m. The required landing distance is mostly influenced by the wing loading and maximum lift coefficient at landing configuration. CHARGE must be able to stop in 60 % of the given maximum LFL. The landing distance is calculated according to RAYMER [20]. The other boundary of the wing loading results from a minimal approach speed $v_{\rm APP,min}$ of International civil aviation organisation (ICAO) approach category C at 121 kts. Any lower approach speed a_{APP} would not be acceptable from an operational perspective. A minimal wing loading can be calculated from the approach speed and maximum lift coefficient in landing configuration $C_{L,max,LDG}$. Again all the landing parameters and the actual landing distance during normal operation are summarised in table 6.

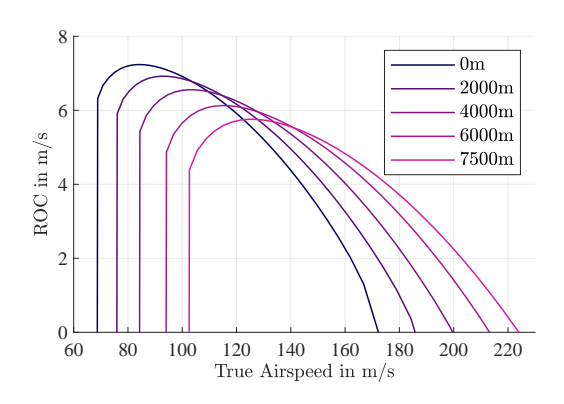


Figure 20 – ROC at different altitudes.

The climb profile of CHARGE is designed to constantly adjust the airspeed to maximum climb speed until the cruise altitude is reached. For the rest of the climb, only $80\,\%$ of the available power is used due to the thermal limitations of the engines. The resulting rate of climb (ROC) at different altitudes is shown in figure 20. All important climb parameters are summarised in table 6.

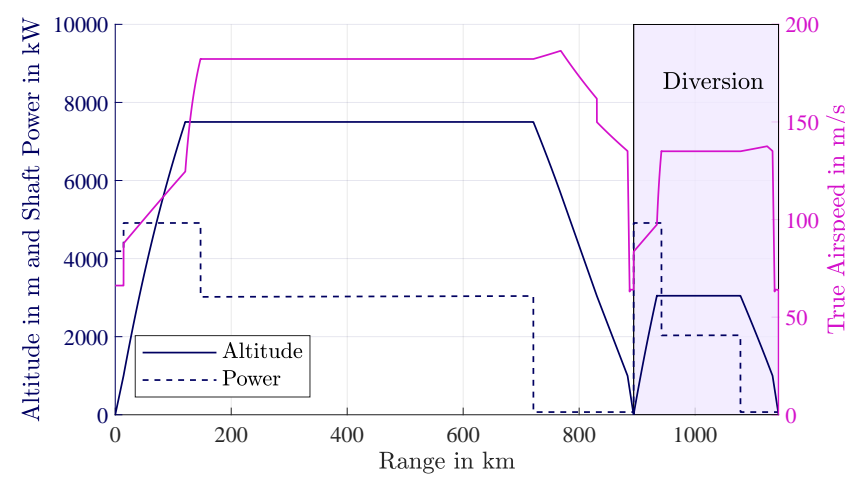


Table 7 – Energy breakdown.

Energy	Share	Energy in kWh	% of $E_{ m tot}$
$E_{ m trip}$	E_{CL}	1,861	25.5
1	$E_{\rm CR}$	2,650	36.3
	$E_{ m des}$	24	0.3
	Σ	4,533	62.1
$E_{ m div}$		1,278	17.5
$E_{ m HLD}$		1,191	16.3
E_{cont}		226	3.1
$E_{ m sys,misc}$		72	1.0
E_{tot}		7,302	100

Figure 21 – Mission profile for design range.

To size the battery of CHARGE a detailed analysis of the required energy is necessary. Besides the major energy percentage used by the propulsion group this includes the EC of all aircraft systems. The calculation follows a simple integration of the varying power consumption over the time of the whole flight mission. Besides the trip energy for the mission range $E_{\rm trip}$ and diversion range $E_{\rm div}$, this includes the energy $E_{\rm HLD}$ for the loitering of $30\,\rm min$ and the contingency energy $E_{\rm cont}$ of $5\,\%$ of the trip energy $E_{\rm trip}$. Figure 21 shows the most important flight parameters over the course of the design mission. An additional $1\,\%$ of the mission energy is added to the total energy $E_{\rm sys,misc}$ to account for all aircraft systems that were not viewed in detail such as the actuation system and avionics. The total energy $E_{\rm tot}$ amounts to $7.3\,\rm MW\,h$ and can be divided into the different flight phases according to table 7.

6. Airplane Operation and Costs

6.1 Operational Concept

To ensure a successful operation on the given flight network, 4 aircraft are required. All aircraft together perform 224 weekly flights with a range between 361 and 894 km and a total of 14 mio. SKO. For the given flight network, an average utilisation of 93% of the passenger capacity and 90% of the aircraft's possible flighttime is achieved. The iteration showed that a cruise speed of Ma 0.57 gives the best economic and environmental design for configuration and operational use. Speeds between Ma 0.5 and Ma 0.6 were considered. Lower speeds are more efficient, but for the given network, Ma 0.57 gives an optimal balance between environmental efficiency and aircraft utilisation. The individual flight information for the design missions are shown in table 8.

CHARGE is equipped with an electric nose landing gear driving system [54]. This speeds up the ground operations and ensures, that taxi in and out times do not exceed the average times given by a report from EUROCONTROL [55]. While the average taxi in time of 4.25 min is already optimised, the average taxi out time of 8.75 min can be further improved with the electric nose landing gear drive system. The aircraft does not need a tug vehicle as it can taxi backwards by itself and can immediately begin to taxi out. Upon arrival at the ramp the aircraft's integrated stairs are immediately extended. The airstairs are already in use today and represent a reasonable compromise between the extra mass carried and a significant reduction in time spent on the ground [54]. Simultaneously the ground crew connects the 4 charging plugs that can charge each battery pack simultaneously. The charging time amounts $12 \min$ to $26 \min$, depending on the mission range.

As the battery degrades over time, it requires replacement after 1,500 full charging cycles. As the

Table 8 - Design missions.

Connection	Range in km	Weekly Flights per Direction	Average PAX	Flight Time in min	Trip Energy in MW h	EC in W h/PAX km
GOT - VBY	361	7	107	43	2.02	52
HAM - RTM	419	3	76	49	2.14	67
HAM - ANR	464	2	89	55	2.41	58
HAM - GOT	471	10	104	56	2.54	52
HAM - PRG	490	8	103	57	2.62	52
HAM - LUX	517	4	89	60	2.65	58
HAM - MUC	601	12	105	68	3.14	50
HAM - SVG	643	5	100	71	3.29	51
HAM - BGO	795	6	93	85	3.91	53
GOT - UME	808	6	106	87	4.09	48
HAM - EDI	894	9	100	94	4.42	49
HAM - TRF TRF - TRD	478 619	5	109	57 69	2.61 3.26	50 48
HAM - FDH FDH - MRS	578 665	6	98	65 73	2.98 3.37	53 52
HAM - SZG SZG - SJJ	605 683	5	107	68 75	3.17 3.53	49 48
BRI - SZG SZG - HAM	799 683	4	108	86 75	4.07 3.54	47 48

flight network includes shorter ranges and ideally avoids using the reserves, the average flight consumes only 25% of a full charge cycle. The partial cycle is not calculated from the percentage of the SOC, but rather from the percentage of charging time $t_{\rm charge,full}$. This ensures a more accurate mapping of the degradation. The cycles are determined as follows:

Cycle [%] =
$$\frac{t_{\text{charge}}}{t_{\text{charge,full}}} \cdot 100$$
 (12)

Consequently, each battery has an estimated lifespan of 23 months. Two access panels on the starboard side of the plane are used for battery replacement. Changing the batteries can be done during a typical C-check. Another operational feature of CHARGE is the single pilot operation system. This can reduce the crew costs by 31%. The pilot can either monitor automated procedures, or steer the aircraft manually. In case of an emergency, it is possible to connect the aircraft to a ground operation station.

6.2 Payload-Range Diagram

The Payload-Range diagram for CHARGE is shown in figure 23. It should be noted that the MLM increases by up to $0.61\,\mathrm{t}$ as the range increases. However, the MTOM remains the same with increasing range, as the aircraft always carries the same battery mass. The fixed battery mass prevents a short-term range extension, such as substituting PAX with fuel. Range extensions can only be achieved, if batteries develop higher energy densities during the 20 years of operation or by carrying less PAX. CHARGE has a ferry range of 1,430 km.

6.3 Environmental and Cost Efficiencies

The cost analysis is performed for a period of 20 years using Thorrow method [56] and 2019 as a reference year for the \$. Due to the unconventional concept, some adjustments need to be made to this method. As the battery degradation is route dependent, battery costs will be initially added once to the capital costs and subsequently added in percentage to the maintenance costs for each flight. After 1,500 completed cycles of the Li-Air batteries, the required SE is no longer given. The batteries can still be used for numerous second life applications [57]. Thus, the following purchase

costs of the batteries are assumed to be $50\,\%$ of the initial battery costs of $200\,\$_{2019}$ kwh. The time between overhaul for electric propulsion systems is 10 times as high as conventional engines, thus the maintenance costs for engines will be reduced by 90% [20]. A single pilot operation enables a $31\,\%$ reduction of the crew costs, thus the SKC are reduced by $0.46\,\$_{2019}$ - Cent, approprimately 6%. A breakdown of the DOC for the given network is shown in figure 22. CHARGE achieves an average SKC of $7.09\,\$_{2019}$ - Cent and an EC of $50.6\,\%_{/kg}$ per PAX.

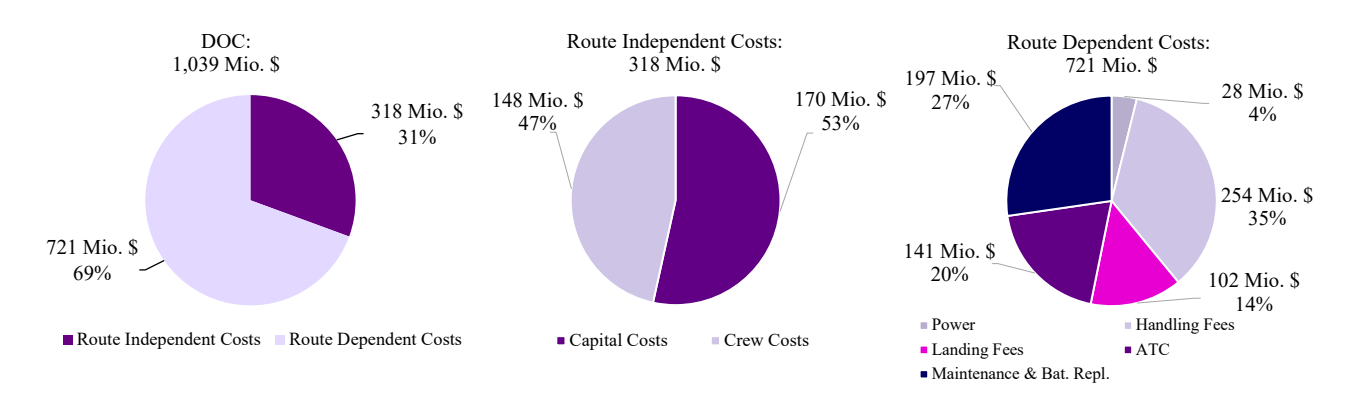


Figure 22 – Breakdown of DOC for operational time of 20 Years.

Figure 24 shows the SKC and EC for CHARGE compared to the Dash 8 [58]. The DOC and EC are shown for fully loaded aircraft as a function of the range. The marked points show CHARGE's performance for the average network given, they are slightly higher due to lower utilisation. CHARGE achieves up to 20 % lower SKC on the given network and consumes 80 % less than Dash 8's energy. However, the comparison should be treated with caution, as kerosene and energy consumption can only be compared with the lower heating value for SAF of 43.2171 M/kg. When comparing costs, it should be noted that the Dash 8 has a longer design range than CHARGE.

The price per kWh for electricity of $0.038\ \$_{2019}$ in 2050 is expected to be significantly lower than for SAF with $0.104\ \$_{2019}$, additionally the grid to shaft efficiency is more than 5 times higher as shown in table 1. The maintenance costs for CHARGE are approximately $150\ \text{Mio}$. $\$_{2019}$ lower than for the Dash 8, due to the electric propulsion. The reduced maintenance and energy costs of CHARGE, both of which depend on the route, combined with the reduced crew costs, result in CHARGE being more economical to operate, even though the initial capital cost is relatively high.

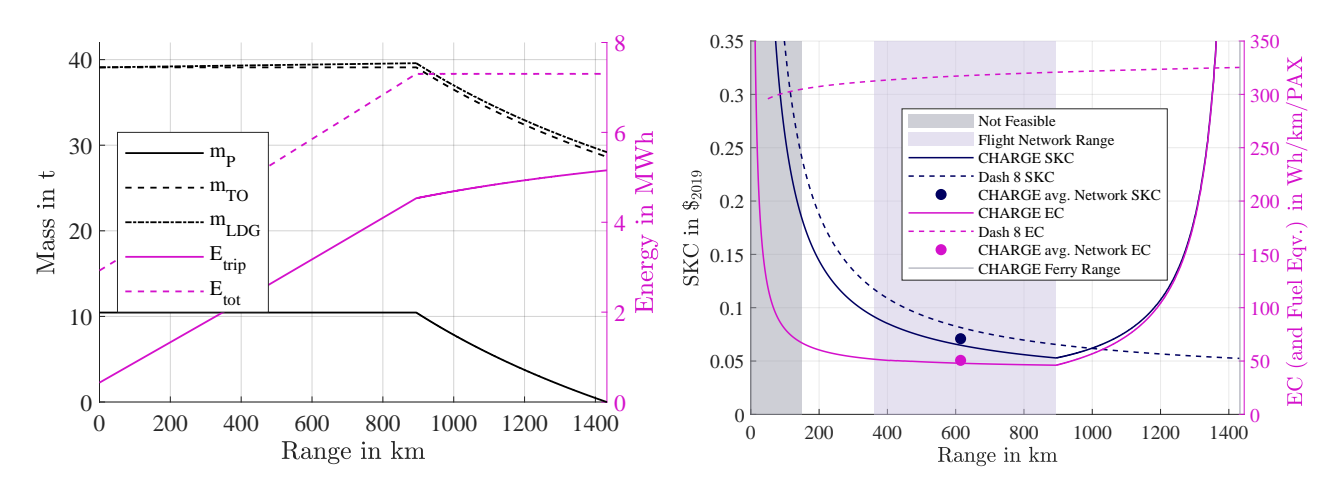


Figure 23 - Payload-range diagram.

Figure 24 - SKC, EC for CHARGE and Dash 8.

7. Iteration and Optimisation

In this years design challenge the assignment is to design an aircraft to operate on a given network in the most efficient way possible taking cost and energy usage into account. In order to fulfil this assignment, it was necessary to set up an iterative design loop to estimate the costs of different abreast and PAX configurations for both direct and indirect route networks. As a consequence, the iterative design loop was used to create not only a single configuration of CHARGE, but also multiple valid configurations and calculate the energy usage and operating costs for the given route network. This can be seen on diagram 5, where all the calculated configurations for both indirect and direct flights are evaluated to identify the optimal solution in accordance with the selected optimising factors for energy and costs.

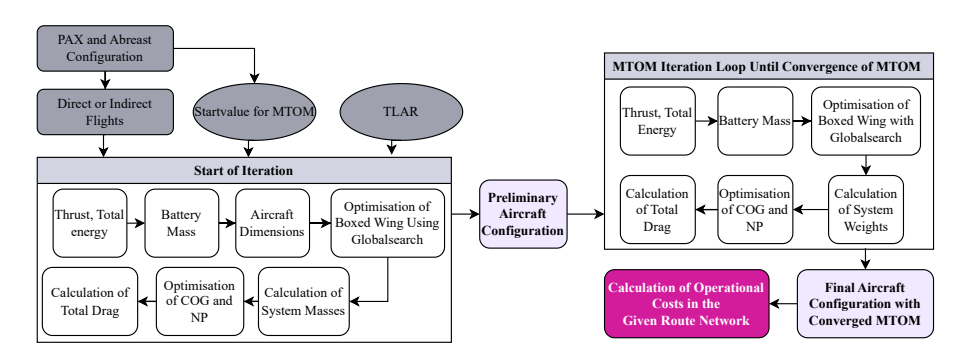


Figure 25 – Diagram of the MATLAB iteration loop.

As shown in figure 25, the calculation of the aircraft configuration contains two main steps. Firstly, the preliminary configuration is calculated with the input values for the initial MTOM, the cabin configuration and top level aircraft requirements (TLAR). In this step, the geometry of the wing is thoroughly optimised using the "globalsearch" algorithm to change all the parameters of the wing in a predefined range. In the second step of the iteration the same steps are calculated as before until the MTOM value has converged. In this step, the wing optimisation is less complex and the wing is only scaled to accommodate the change in MTOM and the horizontal stagger is adjusted to optimise the location of the wing. Once a valid configuration has reached the end of the optimisation algorithm the DOC and EC are calculated based on either the direct and indirect route network selected at the beginning. These values serve a basis for the scoring calculation and the figure 5.

8. Discussion and Conclusion

As demonstrated in preceding sections, electricity represents the optimal source of power for an aircraft engaged in short-haul operations. Although battery technology is not yet sufficiently advanced to enable the production of fully electric aircraft, it is likely to be adequately advanced by an EIS in 2050. This will provide another potential avenue for future development. It is unlikely that alternative technologies such as SAF or hydrogen-powered aircraft will ever be able to fly beyond their initial design range, whereas CHARGE will be able to fly further as soon as battery technology improves. Another benefit of a fully electric aircraft is the reduced environmental impact and economic cost as, electricity is a more cost-effective option compared to SAF or hydrogen alternatives. The selected Li-Air batteries are straightforward to integrate into the aircraft system and promise comparable safety profiles to conventional lithium-ion batteries, given the absence of self-inflammation. If all provided power is generated in an emission-free manner, CHARGE's operation will be entirely carbon neutral. Given that turnaround times at airports can be reduced to a finite limit, as discussed in chapter 6, the charging time is not a significant factor in this concept. This allows for the seamless integration of aircraft into airline fleets and the operation of planes on regional routes.

The chosen BW configuration, in combination with the DEP enables a quiet and efficient flight for regional and domestic operations. Furthermore, the wing area is divided into two smaller sections instead of one large one, resulting in a notable reduction in the dimensions of CHARGE and enhanced operational suitability at smaller regional airports. To reduce turnaround time at airports and thus decrease operational costs for the airline, as well as provide independence from airport infrastructure, the motor, built into the front gear, plays an important role. The numerous small propellers provide a consistent airflow around the wings, thereby enhancing take-off performance and resulting in a noticeably shorter take-off distance than that of the comparable Dash 8. Moreover, the highly efficient electric system and the efficient grid-to-shaft ratio of electricity, as illustrated in table 1, contribute to

the aircraft's capacity to attain an extremely low EC. A substantial contribution to the realisation of this performance is made by the selected motors, powering the propellers, which have been the subject of comprehensive research at NASA and are capable of achieving efficiencies in excess of 99%. This enables CHARGE to achieve a tank-to-shaft efficiency of over 93%.

In conclusion, it can be stated that an electric aircraft like CHARGE represents the optimal solution for regional and short-haul flights, while satisfying all required performance parameters. It is more climate friendly and, despite its innovative nature, is still more cost-effective to operate than other comparable state-of-the-art aircraft.

9. Contact Author Email Address

Clemens Ehrich, clemens.ehrich@gmx.de Luca Kriebel, I.kriebel@tu-berlin.de Tim Schulz, tim.schulz@campus.tu-berlin.de Mathias Tekkel, mathiastekkel@gmail.com Lennart Wauer, wauer@campus.tu-berlin.de Leonid Wenz, leonid.wenz@campus.tu-berlin.de For information about the DLR Design Challenge: Lucas Kugler, lucas.kugler@dlr.de Simon Müller, s.mueller@dlr.de Claudio Niro, claudio.niro@dlr.de

10. Copyright Statement

The authors confirm that they, and/or their company or organization, hold copyright on all of the original material included in this paper. The authors also confirm that they have obtained permission, from the copyright holder of any third party material included in this paper, to publish it as part of their paper. The authors confirm that they give permission, or have obtained permission from the copyright holder of this paper, for the publication and distribution of this paper as part of the ICAS proceedings or as individual off-prints from the proceedings.

References

- [1] L. Kugler, S. Müller, and C. Niro. *DLR Design Challenge*. URL: https://www.dlr.de/en/careers-and-education/research-and-promotion/dlr-design-challenge.
- [2] Deutsches Zentrum für Luft- und Raumfahrt (DLR). DEPA 2050: Development Pathways for Aviation up to 2050. Final Report. 2021.
- [3] J. Begli et al. *DLR Design Challenge 2024 Zukünftige Mobilität auf der Kurzstrecke*. URL: https://www.dlr.de/de/aktuelles/nachrichten/2024/dlr-design-challenge-2024-zukuenftige-mobilitaet-auf-der-kurzstrecke.
- [4] J. Hoidis et al. *DLR awards students for climate-compatible short-haul aircraft*. URL: https://www.dlr.de/en/latest/news/2024/dlr-awards-students-for-climate-compatible-short-haul-aircraft.
- [5] AIRBUS. *Global Market Forecast 2023*. Toulouse, June 2023.
- [6] Juliane Bopst et al. "Wohin geht die Reise? Luftverkehr der Zukunft: umwelt- und klimaschonend, treibhausgasneutral, lärmarm". In: *Umweltbundesamt* (Nov. 2019).
- [7] ReFuelEU Aviation European Commission. URL: https://transport.ec.europa.eu/transport-modes/air/environment/refueleu-aviation_en.
- [8] Regulation (EU) 2023/2405 of the European Parliament and of the Council of 18 October 2023 on ensuring a level playing field for sustainable air transport (ReFuelEU Aviation). Legislative Body: CONSIL, EP. Oct. 2023.
- [9] Global Energy Transition A Roadmap to 2050. Tech. rep. Apr. 2018.
- [10] Alex Schmitt. EU Energy Outlook 2050: How will the European electricity market develop over the next 30 years? Apr. 2022.
- [11] Reynard de Vries et al. "A New Perspective on Battery-Electric Aviation, Part II: Conceptual Design of a 90-Seater". In: Jan. 2024.
- [12] Lilium. URL: https://jet.lilium.com/.
- [13] X-57 Maxwell Overview NASA. Section: Armstrong Flight Research Center. Sept. 2018.

- [14] Michal Janovec et al. "Performance and Weight Parameters Calculation for Hydrogen- and Battery-Powered Aircraft Concepts". In: *Aerospace* 10.5 (May 2023). Publisher: Multidisciplinary Digital Publishing Institute.
- [15] Martin Hepperle. "Electric Flight Potential and Limitations". In: Oct. 2012.
- [16] L. Prandtl. Induced drag of multiplanes. Feb. 1924.
- [17] Giuseppe Palaia, Karim Abu Salem, and Alessandro A. Quarta. "Comparative Analysis of Hybrid-Electric Regional Aircraft with Tube-and-Wing and Box-Wing Airframes: A Performance Study". In: *Applied Sciences* 13.13 (Jan. 2023).
- [18] ICAO Aerodrome Reference Code | SKYbrary Aviation Safety.
- [19] Egbert Torenbeek. *Synthesis of Subsonic Airplane Design*. Dordrecht: Springer Netherlands, 1982.
- [20] Daniel P. Raymer. *Aircraft design: a conceptual approach*. AIAA education series. Reston, VA: American Institute of Aeronautics and Astronautics, Inc, 2018.
- [21] Leland M. Nicolai and Grant Carichner. *Fundamentals of aircraft and airship design*. AIAA educational series. Reston, VA: American Institute of Aeronautics and Astronautics, 2010.
- [22] Majid T. Fard et al. "Aircraft Distributed Electric Propulsion Technologies—A Review". In: *IEEE Transactions on Transportation Electrification* 8.4 (Dec. 2022).
- [23] Martin Hepperle. Aspects of Distributed Propulsion. Oct. 2016.
- [24] EASA.P.002 Dowty R 408 series propellers | EASA.
- [25] EASA.IM.E.049 Pratt & Whitney Canada PW150 series | EASA.
- [26] Kevin R. Moore and Andrew Ning. "Takeoff and Performance Trade-Offs of Retrofit Distributed Electric Propulsion for Urban Transport". In: *Journal of Aircraft* 56.5 (2019).
- [27] Ralph H. Jansen et al. "High Efficiency Megawatt Motor Conceptual Design". In: Cincinnati, OH, July 2018.
- [28] Matthew G. Granger et al. "Concept Design a 1.4 MW Inverter for Rotor Loss Minimization in a Partially Superconducting Motor". In: Anaheim, CA.
- [29] Mona Ghassemi, Ashkan Barzkar, and Mohammadreza Saghafi. "All-Electric NASA N3-X Air-craft Electric Power Systems". In: IEEE Transactions on Transportation Electrification 8.4 (Dec. 2022).
- [30] Patrick C. Vratny, Holger Kuhn, and Mirko Hornung. "Influences of voltage variations on electric power architectures for hybrid electric aircraft". In: *CEAS Aeronautical Journal* 8.1 (Mar. 2017).
- [31] Ashkan Barzkar and Mona Ghassemi. "Electric Power Systems in More and All Electric Aircraft: A Review". In: *IEEE Access* 8 (2020).
- [32] Smruti Sahoo, Xin Zhao, and Konstantinos Kyprianidis. "A Review of Concepts, Benefits, and Challenges for Future Electrical Propulsion-Based Aircraft". In: *Aerospace* 7.4 (Apr. 2020). Number: 4 Publisher: Multidisciplinary Digital Publishing Institute.
- [33] Angel Recalde et al. "Optimal Voltage for More Electric Aircraft direct current cabling system". In: 2021 IEEE Transportation Electrification Conference & Expo (ITEC). June 2021.
- [34] Andrew A. Woodworth, E. Eugene Shin, and Maricela Lizcano. *High Voltage Insulation for Electrified Aircraft*. Oct. 2018.
- [35] David C. Loder, Andrew Bollman, and Michael J. Armstrong. "Turbo-electric Distributed Aircraft Propulsion: Microgrid Architecture and Evaluation for ECO-150". In: 2018 IEEE Transportation Electrification Conference and Expo (ITEC). June 2018.
- [36] DIN Deutsches Institut f\u00fcr Normung e. V., ed. DIN EN 2853 Luft- und Raumfahrt Strombelastbarkeit von elektrischen Leitungen mit Leiter nach EN 2083; Deutsche und Englische Fassung EN 2853:2005. Oct. 2006.
- [37] G. Girishkumar et al. "Lithium-Air Battery: Promise and Challenges". In: *The Journal of Physical Chemistry Letters* 1.14 (July 2010). Publisher: American Chemical Society.
- [38] Md. Arafat Rahman, Xiaojian Wang, and Cuie Wen. "A review of high energy density lithium—air battery technology". In: *Journal of Applied Electrochemistry* 44.1 (Jan. 2014).
- [39] Venkatasubramanian Viswanathan et al. "The challenges and opportunities of battery-powered flight". In: *Nature* 601.7894 (Jan. 2022). Publisher: Nature Publishing Group.

- [40] Xuanxuan Bi et al. "Rechargeable Zinc-Air versus Lithium-Air Battery: from Fundamental Promises Toward Technological Potentials". In: *Advanced Energy Materials* 14.6 (2024).
- [41] Y. Wang et al. "Energy optimization of aircraft thermal management system". In: CSAA/IET International Conference on Aircraft Utility Systems (AUS 2022). Vol. 2022. Aug. 2022.
- [42] Victor Cavalcanti and Claudia Andrade. "A Trade-off Study of a Bleedless and Conventional Air Conditioning Systems". In: Oct. 2008.
- [43] Jonathan M. Rheaume, Malcolm Macdonald, and Charles E. Lents. "Commercial Hybrid Electric Aircraft Thermal Management System Design, Simulation, and Operation Improvements". In: 2019 AIAA/IEEE Electric Aircraft Technologies Symposium (EATS). Aug. 2019.
- [44] Jeffryes W. Chapman, Hashmatullah Hasseeb, and Sydney Schnulo. "Thermal Management System Design for Electrified Aircraft Propulsion Concepts". In: 2020 AIAA/IEEE Electric Aircraft Technologies Symposium (EATS). Aug. 2020.
- [45] Daniel Schiktanz. "Conceptual Design of a Medium Range Box Wing Aircraft". MA thesis. Hochschule für Angewandte Wissenschaften Hamburg, 2011.
- [46] Finck, R. D. USAF (United States Air Force) Stability and Control DATCOM (Data Compendium). Tech. rep. Apr. 1978.
- [47] D Schiktanz and D Scholz. "Box Wing Fundamentals an Aircraft Design Perspective". In: (2011).
- [48] Emanuele Rizzo. Optimization Methods Applied to the preliminary design of innovative non conventional aircraft configurations. Emanuele Rizzo, 2009.
- [49] Fanklin W. Diederich. A simple approximate method for calculating spanwise lift distributions and aerodynamic influence coefficients. Aug. 1952.
- [50] A Wildschek, T Havar, and K Plötner. "An all-composite, all-electric, morphing trailing edge device for flight control on a blended-wing-body airliner". In: *Proceedings of the Institution of Mechanical Engineers, Part G: Journal of Aerospace Engineering* 224.1 (Jan. 2010).
- [51] Srinivas Vasista et al. "Morphing Wing Droop Nose with Large Deformation: Ground Tests and Lessons Learned". In: Aerospace 6.10 (Oct. 2019). Publisher: Multidisciplinary Digital Publishing Institute.
- [52] Giuseppe Palaia. "Design and performance assessment methodologies for box-wing hybridelectric aircraft from urban to regional transport applications". PhD thesis. Pisa: Università di Pisa.
- [53] Pasquale M. Sforza. *Commercial Airplane Design Principles*. 1st ed. Oxford: Elsevier Inc., 2014.
- [54] F Gomez and D Scholz. "IMPROVEMENTS TO GROUND HANDLING OPERATIONS AND THEIR BENEFITS TO DIRECT OPERATING COSTS". In: (2009).
- [55] Taxi times Winter 2021-2022 | EUROCONTROL. May 2022.
- [56] J Thorbeck. TU Berlin Simplified DOC model. Sept. 2013.
- [57] Jia Woon Lee et al. "Technical feasibility and economics of repurposed electric vehicles batteries for power peak shaving". In: *Journal of Energy Storage* 40 (Aug. 2021).
- [58] Institut für Luft- und Raumfahrt. URL: https://luftbau.ilr.tu-berlin.de/webapps/ #app/directOperatingCosts.